Please cite as,

Kondou, C., Koyama, S., "Thermodynamic Assessment of High-Temperature Heat Pumps Using Low-GWP HFO Refrigerants for Heat Recovery", Int. J. Refrig., 53, 126-141 (May 2015). DOI:10.1016/j.ijrefrig.2014.09.018

Title:

Thermodynamic Assessment of High-Temperature Heat Pumps Using Low-GWP HFO Refrigerants for Heat Recovery

Authors: Chieko Kondou*[1], Shigeru Koyama[1, 2]

Affiliations:

1, Interdisciplinary Graduate School of Engineering Sciences, Kyushu University, 6-1 Kasuga-koen, Kasuga, Fukuoka 816-8580, Japan

2, International Institute for Carbon-Neutral Energy Research (WPI-I2CNER), Kyushu University, 6-10-1, Hakozaki, Higashi-ku, Fukuoka, 812-8581, Japan

* Corresponding author.

Tel.: +81 92 583 7832

Fax: +81 92 583 7833

E-mail address: kondo.chieko.162@m.kyushu-u.ac.jp (C. Kondou)

ABSTRACT

Reducing energy consumption by utilizing heat recovery systems has become increasingly important in industry. This paper presents an exploratory assessment of heat pump type heat recovery systems using environmentally friendly refrigerants. The coefficient of performance (COP) of 4 cycle configurations used to raise the temperature of heat media to 160 °C with a waste heat at 80 °C is calculated and compared for refrigerants R717, R365mfc, R1234ze(E), and R1234ze(Z). A multiple-stage "extraction" cycle drastically reduces the throttling loss and exergy loss in the condensers, resulting in the highest COP for R1234ze(Z). A cascade cycle using R1234ze(Z) and R365mfc has a relatively high COP and provides practical benefits. Even under adverse conditions, the primary energy efficiency is greater than 1.3 when the transmission end efficiency of the electric power generation is 0.37. The assessment demonstrated that high-temperature heat pumps are a promising approach for reducing primary energy consumption for industrial applications.

Keywords; low-GWP, R1234ze(E), R1234ze(Z), high-temperature heat pump, heat recovery

NOMENCLATURE

COP	coefficient of performance	(-)
P	pressure	(Pa)
Q	heat transfer rate	(W)
SC	degree of subcool	(K)
SH	degree of superheat	(K)
T	temperature	(°C)
VC	volumetric capacity	(J m^{-3})

W	power	(W)
h	specific enthalpy	(J kg^{-1})
m	mass flow rate	(kg s^{-1})
s	specific entropy	(J $kg^{-1}K^{-1}$)
η_{compr}	compressor efficiency	(-)
η_{mech}	mechanical efficiency	(-)
η_{motor}	motor efficiency	(-)
η_{pe}	primary energy efficiency	(-)
η_{s}	isentropic efficiency	(-)
ρ	density	(kg m^{-3})

Subscripts

compr	compressor
liftG	gross temperature lift
H	heating
cond	condensation
evap	evaporation
V	vapor
r	refrigerant
H_2O	pressurized water (heat media)
src	heat source (waste heat)

i	inlet
o	outlet
overall	overall
sat	saturation
1 ~ 14	position in cycles shown in Figure 2

Superscripts

GC	gas cooler
cond	condenser
SC	subcooler
evap	evaporator
IH	internal heat exchanger
cascade	cascade condenser

1. Introduction

Steam boilers are often used for the drying process of wood or paint, food processing, the distillation process of drugs or drinks, and the cleaning process of machined components. However, in boiler systems, heat loss from a large steam pipe and the emissions of greenhouse gases from fossil fuel combustion are considerable. In addition, the heat exhaust from these relatively high-temperature processes is not utilized in many cases (e.g., US DOE, 2003). According to the research on USA primary energy usage by Rattner and Garimella (2011), the waste heat from power plants is more than sufficient to satisfy all space heating, water heating, and process heating needs. Nonetheless, large amounts of waste heat energy remain unrecovered because of technical and economic barriers. In the report by the USA Department of Energy (DOE) (2008), these barriers are categorized by the cost (e.g., long payback period), chemical composition (e.g., maintenance costs and material constraints), inaccessibility/transportability of heat sources, and temperature restrictions (e.g., mismatching of heat demands and waste heat sources, material constraints).

A large portion of unrecovered waste heat is low quality, i.e., at temperatures below 200 °C, which is barely within the technical limitation of heat pumps. Therefore, recently, attempts to introduce industrial heat pumps to recover waste heat and reduce primary energy consumption have attracted significant attention (e.g., Jacobs *et al.*, 2010). For these industrial applications, heat pumps are capable of increasing the temperature of the waste heat source to a higher, more useful temperature. For instance, Assaf *et al.* (2010) experimentally evaluated heat pumps for food industries utilizing waste steam of 50 °C to produce process steam of 75 °C. For a discussion on technically challenging to high-temperature heat pumps, Bobling and Bouring (2012) experimentally demonstrated the feasibility and reliability of industrial heat pumps using R245fa, R1234ze(E), R365mfc, R236fa, and R717 to provide heat up to 125 °C. Chamoum *et al.* (2014) developed an industrial heat pump using R712 for heat recovery and numerically simulated the dynamic response during an operation for heating a process fluid up to 130 °C. Exergy efficiencies, COPs, and payback periods were analyzed by Cao *et al.* (2014) for water heaters utilizing waste

heat. On the other hand, in the past, there was a view that the efficiency of a heat pump is inferior to combustion in primary energy conversion (Kew, 1982). To provide an answer to this question, the efficiency of heat pump type heat recovery systems should be assessed in terms of primary energy consumption.

The other concern is the global warming potentials (GWP) of the refrigerants used in heat pump systems. On the basis of the second-law analysis, Cavallini *et al.* (2014) evaluated the performance potential of seven conventional refrigerants, three natural refrigerants (R600a, R290, and R717), and three hydro-fluoro-olefins (R1234yf, R1234ze(E), and R1234ze(Z)). In the past few years, R1234ze(Z) was nominated as a low-GWP alternative to R245fa (GWP_{100} = 858) because of its very similar thermodynamic properties and extremely low-GWP (GWP_{100} < 1) (Brown *et al.*, 2009; Fukuda *et al.*, 2014). Similarly, R1234ze(E) with a GWP_{100} of less than 1 (Myhre et al., 2013), has been nominated as an alternative for R134a (GWP_{100} = 1300). A set of 1200 low-GWP refrigerants with critical temperatures between 300 K and 400 K was assessed by McLinden *et al.* (2014), considering flammability, thermal stability, and toxicity for air conditioners. They concluded that no candidate refrigerant is ideal so far. The surveillance range of the critical temperature can be increased for industrial high-temperature heat pumps.

From the above significance and perspective on the environment benign refrigerants, this study provides a brief thermodynamic assessment as the first screening of refrigerants and a case study to calculate more specifically the performances of the proposed cycle configurations. First, a theoretical coefficient of performance (COP) of a basic heating cycle at condensing temperatures from 80 °C to the critical temperatures are evaluated for several refrigerants. Based on this screening, candidate low-GWP refrigerants with different levels of critical temperature are selected, and four different cycle configurations are proposed for a case study. Second, the COP and primary energy efficiency of these cycles using the selected refrigerants are calculated for the case of raising the temperature of pressurized water as a heat media up to 160 °C with the waste heat at

80 °C. From the calculation results, the characteristic of the proposed cycles and the optimum refrigerant for the target temperature are discussed in this paper.

2. Theoretical performance of the selected refrigerants

Table 1 presents a comparison of the characteristics and properties of the selected refrigerants for industrial high-temperature heat pumps. In Table 1, the refrigerants are listed in the order of their critical temperature, the most important parameter influencing the COP and volumetric capacity (Domanski et al., 2014), from left to right. R1234ze(E), R1234ze(Z), R1233zd(E), and R365mfc are the newly recognized substances as refrigerants. R134a, R717, and R245fa are the conventional refrigerants. R365mfc is a hydrofluorocarbon (HFC) that is used as a foaming agent and aerosol propellant and also for a high-temperature heat pump or organic Rankine cycle (ORC) recently. Because R365mfc has a high-GWP value and is highly flammable, hydrofluoroolefins (HFOs) such as R1234ze(E), R1234ze(Z), and R1233zd(E) were introduced. Specifically, the low-GWP refrigerant R1234ze(E) and the isomer R1234ze(Z) have been vigorously investigated during this decade (Brown *et al.* 2009) as alternatives to R134a and R245fa. The natural refrigerant R717, i.e., ammonia, exhibits excellent thermodynamic properties, as mentioned by many forerunners (e.g., Fleming, 1978; Pearson, 1999) but also exhibits quite strong toxicity. R717 is, therefore, considered only for the non-usage or low-pressure side in this study. R365 has the highest critical temperature among the selected refrigerants. Although R365mfc is flammable and has a relatively high-GWP, a low-GWP nonflammable alternative with similar physical properties, for example, the blowing agent HFO-1336mzz(Z) (Loh *et al.*, 2010), will likely be found shortly. Table 2 lists the similar low-GWP alternatives that are currently used as the blowing agent.

Bertinat (1985) reported a comparative assessment of 250 potential refrigerants for a high-temperature heat pump condensing at 150 °C. In his report, Bertinat proposed that the most important factors for screening refrigerants is the COP, the specific compressor displacement (SCD), which is the inverse of the volumetric capacity, and the minimum superheat required

to prevent liquid compression. Following Bertinat's work, Figure 1 shows the performance of a theoretical heat pump cycle using the selected refrigerants. Figure 1 (a) illustrates the calculation conditions of a theoretical cycle on the refrigerant *T*-*s* diagram to evaluate the heating COP, COP_H, pressure ratio, P_d/P_s, and volumetric capacity VC_H. Here, the temperature lift, i.e., temperature difference between condensation and evaporation, is fixed at 80 K because the waste heat temperature is most likely subject to being the end-use temperature. The waste heat temperature is decreased when the heat is dissipated in the ambient atmosphere. If the dissipation ratio of waste heat was fixed, the waste heat from a system running at higher temperatures is prone to be a high temperature. Thus, the temperature lift is fixed in this evaluation rather than the evaporation temperature. The temperature lift of 80 K and the subcool of 60 K are significantly larger than those of the typical operation conditions of air conditioners and were used to simulate the operation for the industrial heat pumps for waste heat recovery. The physical properties are calculated using REFPROP 9.1 (Lemmon *et al.*, 2013) coupled with the incorporated coefficients optimized by Akasaka *et al.* (2013). Under the given conditions, the COP_H and VC_H are defined as follows:

$$COP_H = \Delta h_{cond} / \Delta h_{compr}, \quad \text{and} \quad VC_H = \rho_V \Delta h_{cond} \tag{1}$$

In Figures 1 (b), 1 (c), and 1 (d), COP_H, P_d/P_s, and VC_H, respectively, are plotted by varying the condensation temperature from 80 °C to the temperature just below the critical point. As the condensation temperature increases to the critical temperature, the COP monotonically increases. This theoretical COP indicates the possible line of the developments and does not take into account the irreversible losses. The pressure ratio decreases with increasing condensation temperature at the fixed temperature lift because of the increasing evaporation pressure, whereas the volumetric capacity increases because of the decreasing latent heat in the condenser. Under the condition of this large temperature lift of 80 K, the pressure ratio easily exceeds 5. Operating steadily at pressure ratios beyond 5 with a single compression is difficult with the existing technology. When the volumetric capacity is insufficient or far smaller than that of conventional refrigerants such as R134a and R245fa, to maintain the heating capacity with the same size compressor and heat exchangers, the irreversible loss is prone to increase because of the requirement

of a substantially higher refrigerant circulation ratio. To avoid this problem, substantially larger equipment is required; however, the market would not accept this economic burden. To reduce the pressure ratio while increasing the volumetric capacity, selecting a refrigerant to operate at just below the critical temperature at a given condition is very important, and techniques using multiple-stages or cascading would be necessary. For instance, for the cases to provide a heat media of approximately 160 °C, R1234ze(E), R1233zd(E), or R365mfc would be suitable. Based upon this brief assessment, a case study with more specific cycle configurations such as multiple-stages and cascade cycles on a heat recovery system is hereafter discussed.

3. Case study on heat recovery systems upgrading heat from 80 °C to 160 °C

In the following case study, the performance of an industrial heat pump system to recover waste heat is calculated. Utilizing the waste heat of 80 °C, the heat media of pressurized water is preheated to 70 °C. Then, the pressurized water at 1 MPa is heated from 70 °C to 160 °C by a heat pump system and delivers the heat to the usage site. Then, some portion of the pressurized water returns to the entrance of the heat pump system. The heat is dissipated from the usage site to the atmosphere. This waste heat is, of course, used as the heat source of the heat pump.

3.1 Cycle configurations

Figure 2 shows four cycle configurations of the heat pump system for heat recovery. Figures 2 (a), 2 (b), 2 (c), and 2 (d) correspond to the proposed cycles: a triple tandem cycle, two-stage extraction cycle, three-stage extraction cycle, and cascade cycle, respectively. In the triple tandem cycle of Figure 2 (a), an internal heat exchanger is used to reduce the pressure ratio of the third cycle. The extraction cycle shown in Figures 2 (b) and 2 (c) is a unique system to extract the vapor from the compressor. The extracted vapor rejects heat in a condenser, and then it converges with the liquid that flowed through a condenser and an expansion valve on the higher pressure side. After the conversion, the enthalpy and mass flow rate are increased by the liquid

from the higher pressure side, and then the heat is rejected to the pressurized water in a subcooler. By converging the extracted vapor and the liquid from the higher pressure side, the internal energy remaining in the liquid is utilized in the subcooler instead of losing it as the throttling loss in an expansion valve returning to the evaporator. In the cascade cycle of Figure 2 (d), the pressurized water is heated with a subcooler of the bottom cycle (the low-temperature side cycle) and continuously heated in the two-stage extraction cycle of the top cycle (the high-temperature side cycle). In the case where the COP is improved, an internal heat exchanger is applied in the cycles of Figures 2 (c) and 2 (d), as indicated by the dashed line. The triple tandem cycle, two-stage extraction cycle, three-stage extraction cycle, and cascade cycle are denoted as cases I, II, III, and IV, respectively, in this paper.

3.2 Calculation conditions and models for components

3.2.1 Compressor Regardless of the pressure ratio or the rotation speed, the isentropic, mechanical, and motor efficiency are given as 0.92, 0.85, and 0.90, respectively, for each compressor or compression process. The degree of superheat at the compressor suction side is maintained at 5 K. To avoid the wet compression, the degree of superheat is increased excessively by an internal heat exchanger to keep the compressor discharge state superheated.

3.2.2 Evaporator Figure 3 illustrates the calculation model of the temperature distribution in the evaporator and the condenser/gas-cooler/subcooler on the T-Q diagram of the refrigerant. In this model, the pinch temperature (i.e., the minimum approach temperature) is 5 K in the subcool and superheat regions, whereas it is 2 K in the two-phase region. The evaporation pressure is a saturation pressure, which corresponds to the saturation temperature that is 2 K below the outlet temperature of the heat source fluid. The outlet temperature of superheated vapor is 5 K below the inlet temperature of the heat source fluid. As listed in Table 3 and denoted in Figure 2, the waste heat temperature is given as 80 °C and 70 °C at the inlet and outlet of

the evaporator for the standard condition. Therefore, the evaporation temperature (two-phase region) and evaporation outlet temperature (superheated region) of the refrigerant side is unambiguously determined as 68 °C and 75 °C, respectively.

3.2.3 Condenser/Gas-cooler/Subcooler As shown in Figure 3, the condensation pressure is determined as corresponding to a saturation temperature that is 2 K above the outlet temperature of the pressurized water. In the case where the pressure exceeds the critical point, the pressure in the gas cooler is determined with a pinch temperature of 5 K. The gas cooler is partitioned into 10 segments on the basis of the specific entropy change of the refrigerant side, and the pinch temperature is the minimum temperature difference in those segments. For the subcooler, the pinch point that appears either at the entrance or the exit is greater than 5 K. The inlet and outlet temperatures of pressurized water in the condenser/gas cooler/subcooler can be arbitrarily given and then the refrigerant side temperature is unambiguously determined with desired temperature differences. For case I of the triple tandem cycle, the temperature rise in each individual cycle is divided equally, namely, 30 K for each cycle. For cases II, III, and IV, the condenser/gas cooler/subcooler inlet temperatures, denoted as $T_{\mathrm{H2O,i}}^{\mathrm{cond1}}$ or $T_{\mathrm{H2O,i}}^{\mathrm{cond2'}}$ and $T_{\mathrm{H2O,i}}^{\mathrm{cond3}}$ in Figure 2, are optimized to maximize the overall COP and primary energy efficiency.

3.2.4 Internal heat exchanger/Cascade condenser As drawn by the dotted lines in Figure 2, an internal heat exchanger can be considered if it improves the COP or if it is necessary to keep the refrigerant state superheated at the compressor discharge. The pinch point at either the entrance or the exit is always greater than 2 K. Under these conditions, the optimum point of the compressor suction temperature and the heat transfer rate in the internal heat exchanger are iteratively found. In the cascade condenser of case IV, the difference between two saturation temperatures of the top cycle and bottom cycle is set as 5 K. The pinch temperature difference in the cascade condenser of case IV is maintained to be greater than 2 K at either the entrance or the exit.

3.3 Calculation procedure for cases III and IV

3.3.1 Case III: Three-stage extraction cycle

The coefficient of performance (COP) of case III is calculated as follows. The temperature, pressure, specific enthalpy, and specific entropy of the refrigerant circuit are calculated along the numbers appended in Figure 2 (c).

$$1: \quad T_1 = T_{\mathrm{src,o}} + \Delta T_{\mathrm{i}}^{\mathrm{evap}}, \qquad P_1 = P_{\mathrm{sat}}\left(T_1\right), \qquad h_1 = h_{14}, \qquad s_1 = s\left(P_1, h_{14}\right) \tag{1}$$

$$2: \quad T_2 = T_{\mathrm{src,o}} + \Delta T_{\mathrm{o}}^{\mathrm{evap}}, \qquad P_2 = P_1 = P_{\mathrm{sat}}\left(T_1\right), \qquad h_2 = h\left(P_2, T_2\right), \qquad s_2 = s\left(P_1, T_2\right) \tag{2}$$

$$3: \quad T_3 = T_{\mathrm{H2O,o}}^{\mathrm{cond1'}} + \Delta T_{\mathrm{i}}^{\mathrm{cond}}, \qquad P_3 = P_{\mathrm{sat}}\left(T_3\right), \qquad h_3 = h_2 + \Delta h_{\mathrm{compr1}}, \qquad s_3 = s\left(P_3, h_3\right) \tag{3}$$

$$4: \quad T_4 = T\left(P_4, h_4\right), \ P_4 = P_{\mathrm{sat}}\left(T_{\mathrm{H2O,o}}^{\mathrm{cond2}} + \Delta T_{\mathrm{i}}^{\mathrm{cond}}\right) \text{ or } P\left(T_{\mathrm{H2O}}^{\mathrm{cond2}} + \Delta T^{\mathrm{GC}}\right), \ h_4 = h_3 + \Delta h_{\mathrm{compr2}}, \ s_4 = s\left(P_4, h_4\right) \tag{4}$$

$$5: \quad T_5 = T\left(P_5, h_5\right), \ P_5 = P_{\mathrm{sat}}\left(T_{\mathrm{H2O,o}}^{\mathrm{cond3}} + \Delta T_{\mathrm{i}}^{\mathrm{cond}}\right) \text{ or } P\left(T_{\mathrm{H2O}}^{\mathrm{cond3}} + \Delta T^{\mathrm{GC}}\right), \ h_5 = h_4 + \Delta h_{\mathrm{compr3}}, \ s_5 = s\left(P_5, h_5\right) \tag{5}$$

where, $T_{\mathrm{src,o}}$, $\Delta T_{\mathrm{i}}^{\mathrm{evap}}$, $\Delta T_{\mathrm{o}}^{\mathrm{evap}}$, $\Delta T_{\mathrm{i}}^{\mathrm{cond}}$, and ΔT^{GC} are 70 °C, 2 K, 5 K, 2 K, and 5 K, respectively, at the standard conditions, as listed in Table 3. Considering the efficiencies, the shaft power $\Delta h_{\mathrm{compr}}$ and the total power consumption W of the compressors are expressed as,

$$\begin{cases} \Delta h_{\mathrm{compr1}} = \left[h_3'\left(P_3, s_2\right) - h_2 \right] / \eta_{\mathrm{s}} \\ \Delta h_{\mathrm{compr2}} = \left[h_4'\left(P_4, s_3\right) - h_3 \right] / \eta_{\mathrm{s}} \\ \Delta h_{\mathrm{compr3}} = \left[h_5'\left(P_5, s_4\right) - h_4 \right] / \eta_{\mathrm{s}} \end{cases} \tag{6}$$

$$\begin{cases} W_1 = \left(\Delta h_{\mathrm{compr1}} \eta_{\mathrm{mech}} \eta_{\mathrm{motor}}\right) m_{\mathrm{r1}} \\ W_2 = \left(\Delta h_{\mathrm{compr2}} \eta_{\mathrm{mech}} \eta_{\mathrm{motor}}\right)\left(m_{\mathrm{r2}} + m_{\mathrm{r3}}\right) \\ W_3 = \left(\Delta h_{\mathrm{compr3}} \eta_{\mathrm{mech}} \eta_{\mathrm{motor}}\right) m_{\mathrm{r3}} \end{cases} \tag{7}$$

where h_3', h_4', and h_5' denote the isentropic state on s_2, s_3, and s_4, respectively. From number 6 in Figure 2, the refrigerant state of case III is calculated as,

$$6: \quad T_6 = T_{\mathrm{H2O,i}}^{\mathrm{cond3}} + \Delta T_{\mathrm{o}}^{\mathrm{cond}}, \quad P_6 = P_5, \quad h_6 = h_5 - \left(Q_3 / m_{\mathrm{r3}}\right), \quad s_6 = s\left(P_6, h_6\right) \tag{8}$$

$$7: \quad T_7 = T\left(P_7, h_7\right), \quad P_7 = P_4, \quad h_6 = h_7, \quad s_7 = s\left(P_7, h_7\right) \tag{9}$$

$$8: \quad T_8 = T\left(P_8, h_8\right), \quad P_8 = P_4, \quad h_8 = h_4 - Q_2 / m_{\mathrm{r2}}, \quad s_8 = s\left(P_8, h_8\right) \tag{10}$$

$$9: \quad T_9 = T\left(P_9, h_9\right), \quad P_9 = P_4, \quad h_9 = \frac{\left(h_8 m_{\mathrm{r2}} + h_7 m_{\mathrm{r3}}\right)}{\left(m_{\mathrm{r2}} + m_{\mathrm{r3}}\right)}, \quad s_9 = s\left(P_9, h_9\right) \tag{11}$$

$$10: \quad T_{10} = T_{\mathrm{H2O,i}}^{\mathrm{cond2'}} + \Delta T_{\mathrm{o}}^{\mathrm{cond}}, \quad P_{10} = P_4, \quad h_{10} = h_9 - \frac{Q_2'}{\left(m_{\mathrm{r2}} + m_{\mathrm{r3}}\right)}, \quad s_{10} = s\left(P_{10}, h_{10}\right) \tag{12}$$

11: $T_{11} = T\left(P_{11}, h_{11}\right),\quad P_{11} = P_3,\quad h_{11} = h_{10},\quad s_{11} = s\left(P_{11}, h_{11}\right)$ (13)

12: $T_{12} = T\left(P_{12}, h_{12}\right),\quad P_{12} = P_3,\quad h_{12} = h_3 - Q_1/m_{r1},\quad s_{12} = s\left(P_{12}, h_{12}\right)$ (14)

13: $T_{13} = T\left(P_{13}, h_{13}\right),\quad P_{13} = P_3,\quad h_{13} = \dfrac{\left[h_{12}m_{r1} + h_{11}\left(m_{r2} + m_{r3}\right)\right]}{\left(m_{r1} + m_{r2} + m_{r3}\right)},\quad s_{13} = s\left(P_{13}, h_{13}\right)$ (15)

14: $T_{14} = T_{H2O,i}^{cond1'} + \Delta T_o^{cond},\quad P_{14} = P_3,\quad h_{14} = h_{13} - \dfrac{Q_1'}{\left(m_{r1} + m_{r2} + m_{r3}\right)},\quad s_{14} = s\left(P_{14}, h_{14}\right)$ (16)

When the inlet temperatures of the pressurized water in the heat exchangers 2' and 3 of heat transfer rates Q_2'and Q_3, respectively, are given, the state of this cycle is determined to satisfy the following heat balances.

$$\begin{cases} Q_1' = \left[h_{H2O}\left(T_{H2O,i}^{cond1}\right) - h_{H2O}\left(T_{H2O,i}\right)\right]m_{H2O} = \left(h_{14} - h_{13}\right)\left(m_{r3} + m_{r2} + m_{r1}\right) \\ Q_1 = \left[h_{H2O}\left(T_{H2O,i}^{cond2'}\right) - h_{H2O}\left(T_{H2O,i}^{cond1}\right)\right]m_{H2O} = \left(h_3 - h_{12}\right)m_{r1} \\ Q_2' = \left[h_{H2O}\left(T_{H2O,i}^{cond2}\right) - h_{H2O}\left(T_{H2O,i}^{cond2'}\right)\right]m_{H2O} = \left(h_9 - h_{10}\right)\left(m_{r3} + m_{r2}\right) \\ Q_2 = \left[h_{H2O}\left(T_{H2O,i}^{cond3}\right) - h_{H2O}\left(T_{H2O,i}^{cond2}\right)\right]m_{H2O} = \left(h_4 - h_8\right)m_{r2} \\ Q_3 = \left[h_{H2O}\left(T_{H2O,o}\right) - h_{H2O}\left(T_{H2O,i}^{cond3}\right)\right]m_{H2O} = \left(h_5 - h_6\right)m_{r3} \end{cases} \quad (17)$$

$$\begin{cases} T_{H2O,i} = T_{H2O,i}^{cond1'}\left(= 70\ ^{o}C\right) \\ T_{H2O,o}^{cond1'} = T_{H2O,i}^{cond1},\quad T_{H2O,o}^{cond1} = T_{H2O,i}^{cond2'} \\ T_{H2O,o}^{cond2'} = T_{H2O,i}^{cond2},\quad T_{H2O,o}^{cond2} = T_{H2O,i}^{cond3} \\ T_{H2O,o} = T_{H2O,o}^{cond3}\left(= 160\ ^{o}C\right) \end{cases} \quad (18)$$

With a given heat load (Q_1'+Q_1+Q_2'+Q_2+Q_3) and the pressurized water temperatures $T_{H2O,i}^{cond2'}$ and $T_{H2O,i}^{cond3}$, the remaining pressurized water temperature $T_{H2O,i}^{cond1}$ and the refrigerant mass flow rates m_{r1}, m_{r2}, and m_{r3} are iteratively obtained. Thus, the overall COP of the heating cycle of case III is,

$$\left(COP_H\right)_{overall} = \frac{Q_1' + Q_1 + Q_2' + Q_2 + Q_3}{W_1 + W_2 + W_3} \quad (19)$$

By sequentially varying the parameters $T_{H2O,i}^{cond2'}$ and $T_{H2O,i}^{cond3}$, the combinations to maximize the overall COP are found for case III.

3.3.2 Case IV: Cascade cycle

For the cascade cycle case IV, the compression work per unit refrigerant mass Δh_{compr} and the power consumption W in

the compressors are,

$$\begin{cases} \Delta h_{\text{compr1}} = \left[h_3'\left(P_3, s_2\right) - h_2 \right] / \eta_{\text{s}} \\ \Delta h_{\text{compr2}} = \left[h_8'\left(P_8, s_7\right) - h_7 \right] / \eta_{\text{s}} \\ \Delta h_{\text{compr3}} = \left[h_9'\left(P_9, s_8\right) - h_8 \right] / \eta_{\text{s}} \end{cases} \tag{20}$$

$$\begin{cases} W_1 = \left(\Delta h_{\text{compr1}} \eta_{\text{mech}} \eta_{\text{motor}} \right) m_{\text{r1}} \\ W_2 = \left(\Delta h_{\text{compr2}} \eta_{\text{mech}} \eta_{\text{motor}} \right) \left(m_{\text{r2}} + m_{\text{r3}} \right) \\ W_3 = \left(\Delta h_{\text{compr3}} \eta_{\text{mech}} \eta_{\text{motor}} \right) m_{\text{r3}} \end{cases} \tag{21}$$

The cycle state is determined when the inlet temperatures of the pressurized water in the heat exchangers 2' and 3, $T_{\text{H2O,i}}^{\text{cond2}'}$ and $T_{\text{H2O,i}}^{\text{cond3}}$, respectively, are given to satisfy the following heat balances.

$$\begin{cases} Q_1' = \left[h_{\text{H2O}}\left(T_{\text{H2O,i}}^{\text{cond1}}\right) - h_{\text{H2O}}\left(T_{\text{H2O,i}}\right) \right] m_{\text{H2O}} = \left(h_4 - h_5\right) m_{\text{r1}} \\ Q_2' = \left[h_{\text{H2O}}\left(T_{\text{H2O,i}}^{\text{cond2}}\right) - h_{\text{H2O}}\left(T_{\text{H2O,i}}^{\text{cond2}'}\right) \right] m_{\text{H2O}} = \left(h_{13} - h_{14}\right)\left(m_{\text{r3}} + m_{\text{r2}}\right) \\ Q_2 = \left[h_{\text{H2O}}\left(T_{\text{H2O,i}}^{\text{cond3}}\right) - h_{\text{H2O}}\left(T_{\text{H2O,i}}^{\text{cond2}}\right) \right] m_{\text{H2O}} = \left(h_8 - h_{12}\right) m_{\text{r2}} \\ Q_3 = \left[h_{\text{H2O}}\left(T_{\text{H2O,o}}\right) - h_{\text{H2O}}\left(T_{\text{H2O,i}}^{\text{cond3}}\right) \right] m_{\text{H2O}} = \left(h_9 - h_{10}\right) m_{\text{r3}} \end{cases} \tag{22}$$

In addition, in the cascade condenser, the following heat balance is maintained:

$$Q_1 = \left(h_3 - h_4\right) m_{\text{r1}} = \left(h_7 - h_6\right)\left(m_{\text{r2}} + m_{\text{r3}}\right) \tag{23}$$

The temperatures in the above heat balances and also the temperatures relating to the cascade condensers are given as,

$$\begin{cases} T_{\text{H2O,i}} = T_{\text{H2O,i}}^{\text{cond1}'} \left(= 70\ ^{\circ}\text{C}\right) \\ T_{\text{H2O,o}}^{\text{cond1}'} = T_{\text{H2O,i}}^{\text{cond2}'},\ T_{\text{H2O,o}}^{\text{cond2}'} = T_{\text{H2O,i}}^{\text{cond2}},\ T_{\text{H2O,o}}^{\text{cond2}} = T_{\text{H2O,i}}^{\text{cond3}} \\ T_{\text{H2O,o}} = T_{\text{H2O,o}}^{\text{cond3}} \left(= 160\ ^{\circ}\text{C}\right) \end{cases} \tag{24}$$

$$\begin{cases} T_{\text{cond}}^{\text{cascade}} - T_{\text{eva}}^{\text{cascade}} = T_4 - T_6 = 5\ \text{K} \\ T_3 - T_7 = 2\ \text{K} \end{cases} \tag{25}$$

From the above conditions, the refrigerant mass flow rates are determined at a given heat load. Thus, the overall COP of the heating cycle of case IV is,

$$\left(COP_{\text{H}}\right)_{\text{overall}} = \frac{Q_1' + Q_2' + Q_2 + Q_3}{W_1 + W_2 + W_3} \tag{26}$$

The temperatures $T_{\text{H2O,i}}^{\text{cond2}'}$ and $T_{\text{H2O,i}}^{\text{cond3}}$ in Eq. (24) are optimized to maximize the overall COP of Eq. (26).

3.4 Calculation results for the target temperature of 160 °C with the typical conditions

Table 4 lists the calculation results of the overall COP and supplementary information: the change in the pressurized water temperature, refrigerants, COP, volumetric capacity, pressure ratio of the individual value, or the name for each stage. The left column shows the state of the low-temperature side cycle or bottom cycle; right columns. Hence, the temperature rise of pressurized water through each stage, refrigerant, COP, volumetric heating capacity, and pressure ratio in each individual cycle is listed in each column. For instance, in case I, R1234ze(E), R1234ze(Z), and R365mfc were used for low, medium, and high-temperature side cycles, respectively. For case IV-b, R717 and R365mfc were used for bottom and top cycles, respectively. Then, the pressure ratio of the high-side stage in the top cycle is 1.93. The performance is also expressed in terms of the primary energy efficiency, assuming a transmission end efficiency of electric power generation of 0.37. As listed in Table 4, all of the primary energy efficiencies are above 1.0, which indicates positive perspectives for the reduction of primary energy consumption by using the heat pump type heat recovery systems. Figures 4, 5, and 6 are *P-h* and *T-s* diagrams that show the calculation results for the high-temperature heat pump cycles of cases I, III, and IV, respectively. The thick solid line indicates the state of the refrigerant along with numbers corresponding to those states in Figure 2. The other two thin solid lines in the *T-s* diagrams indicate the temperature of the pressurized water and heat source fluid as addressed to the refrigerant state. It should be noted that the horizontal axis corresponds to the specific entropy of the refrigerant but not to the water or heat source fluid. The temperatures of the pressurized water and heat source correspond to the refrigerant state.

Figure 4 plots the results of the triple tandem cycle applying R1234ze(E), R1234ze(Z), and R365mfc for the low, medium, and high sides, respectively. A major concern is the large pressure ratio of the high-side cycle. As a consequence of the large throttling loss due to the large pressure ratio 8.43 (P_d/P_s = 8.43 as listed in Table 4), the overall COP decreases. To reduce the throttling loss, a momentum recovery using an ejector or expander could be a possible solution. This solution would result in an additional step in the development, even though this cycle has the advantage of easy control by the independent stages. In

the cycle of R365mfc, a large superheat is required to keep the compressor discharge state superheated by using the internal heat exchanger. For applying these refrigerants having the large isentropic exponent, an additional component such as the internal heat exchanger may be necessary to avoid wet compression.

Cases II and III of the multiple-stage extraction cycle achieve a substantially higher COP than that of the tandem cycle. When R1234ze(Z) and R365mfc are applied in the two-stage extraction cycle (case II) as listed in Table 4, the overall COP is 4.83. When either R1234ze(Z) or R365mfc is applied in the three-stage extraction cycle (cases III-a or III-b), the COP is 4.94 or 4.84. In particular, for the three-stage extraction cycle, the pressure ratio of each stage is reduced below three. This reduction has a significant benefit of reducing the throttling loss in the expansion valves and the mechanical fatigue in the compressors. The reduction of the throttling loss is illustrated in Figure 5 (b) with the short line segment 6-7 and also in Figure 6 (b) over the short line segments of 6-7, 10-11, and 14-1. In addition, by utilizing the subcoolers, the irreversible loss of heat transfer is reduced. In the extraction cycle, the extracted vapor rejects the heat once in the condenser and then converges with the refrigerant flow from the high-pressure side, which is somewhat flashed in the expansion valve. Thus, the internal energy of the refrigerant flow is transferred to the pressurized water as much as possible rather than wasted in the expansion valve. The reduced irreversible loss is illustrated in Figure 6 (b) by the line indicating the pressurized water temperature bending up to the refrigerant temperature of the line segments 4-7-8-9-10 and 3-11-12-13-14. Comparing the overall COP between cases III-a and III-b, the COP of case III-a is slightly higher than the COP of the other cases. The critical temperature, where the theoretical COP and volumetric capacity are nearly maximized, R1234ze(Z) is closer to the target temperature of the outlet pressurized water. Most likely, this critical temperature value makes the use of R1234ze(Z) advantageous in the cycle. In addition, as shown in Figure 8 (a), the reduction in the COP with changes in the operation conditions is moderate, which means that this cycle could achieve the designed stable performance. The above-mentioned thermodynamic attraction is significant; nevertheless, an issue for the development of the heat pump system remains. These multiple-stage cycles do not allow the individual control of

each stage, which makes cycle control very difficult. To solve this problem partially, a cascade cycle is suggested.

For the cascade cycle of case IV, the states of the bottom cycle (the low-temperature side) and top cycle (the high-temperature side) are drawn by the dashed and solid lines in Figure 7. The irreversible loss due to the heat transfer is additionally generated in the cascade condenser, as illustrated by the area in between the solid line 6-7 and the dashed line 3-4. As a consequence of the heat transfer loss, at the condensing temperature in the cascade condenser of 117 °C, the overall COP of the cascade cycle of case IV-a, applying R1234ze(Z) for the bottom cycle and R365mfc for the top cycle, is 4.68, which is somewhat lower than that of the multiple-stage extraction cycles. As shown in Figure 8 (b), the overall COP of case IV decreases more than that of case III-a. The heat transfer loss in the cascade condenser can be increased according to the operation conditions, which does not occur in case III-a. Thus, the overall COP can be decreased considerably. However, individual control is allowed for the top and bottom cycles, and it makes the load adjustment and operation optimization considerably easier. The cascade cycle provides some other practical benefits. For example, the individual start and refrigerant selection of the bottom cycle can protect the compressors from the "liquid back" at the cold start. The lubricant oil can be selected for the particular temperature range of each stage. In addition, if a refrigerant possessing large volumetric capacity is used for the bottom cycle, then the downsizing of the compressor and some other parts of the heat pump can be achieved. Case IV-b is a cascade cycle applying R717 (i.e., ammonia) for the bottom cycle instead of R1234ze(Z), as listed in Table 4. The volumetric capacity of R717 at the bottom cycle is 5.23, which is 1.76 times that of the R1234ze(Z). This volumetric heating capacity allows for the drastic downsizing of the heat pump unit and, most likely, the reduction in the irreversible loss by the pressure drop. Although the calculation result suggests a slightly lower overall COP with R717 than with R1234ze(Z), the reversal pattern of the COP is possible in reality.

3.5 Effects of the compressor and heat exchanger performance on the COP

Table 5 presents the effects of the compressor efficiency and heat exchanger size on the overall COP to set the lowest limit of development for these components. The variations in the overall COP of cases II, III-a, and IV-a are listed in Table 5. The conditions are gradually changed in the following steps. First, lowering the isentropic compression efficiency to values of 0.92, 0.85, and 0.80, which is equivalent to the overall efficiency of the compressor of 0.70, 0.65, and 0.61, respectively. Second, increase the pinch temperature differences in the condenser and evaporator from 2 K to 5 K and 8 K, respectively. Similarly, at the condenser outlet, the temperature difference is increased from 5 K to 8 K. With the first change in the isentropic compression efficiency, the overall COP decreases by approximately 11%. With the increased temperature difference in the heat exchangers, the COP decreases by approximately 22% to 24%. The reason why the COP of cases III-a and IV-a decrease more severely than the others is simply that many more heat exchangers are built into the cycles of cases III and IV.

Figure 9 shows the state of cycle III-a changing with the change in the compressor efficiency. As the isentropic efficiency η_s decreases, the lines showing the compression process leans further and the degree of superheat at the compressor discharge increases. This suggests a deviation from the isentropic lines and an increase in the compression work. Figure 10 shows the additional change in the state of cycle III-a under the more adverse condition. With an increase in the temperature differences, the pressure ratio of the first compression process increases notably. In this process, the refrigerant mass flow rate is the greatest, and the increase in the pressure ratio severely influences the COP. Because the isentropic compression work is generally larger at lower pressures, the decrease in the evaporation pressure decreases the COP even more.

Likewise, the COP decreases along with the gradually adverse conditions, and the primary energy efficiency decreases as well. At the worst conditions, the primary energy efficiencies are 1.38 to 1.51, which are still sufficiently in excess of the criteria 1.0. Thus, once the assumed limit of development was achieved for a compressor and heat exchanger, these high-temperature heat pumps became advantageous over combustion boilers in terms of the energy consumption.

3.6 Effects of the waste heat amount and heat recovery rate on the COP

Another major concern in the feasibility assessment is the balance of the waste heat amount and the heating load of the heat pumps. Ideally, if 100% of the waste heat was recovered, the heat pump systems could circulate the heat in a system perfectly, and other heating systems would technically be unnecessary. After complete removal of the waste heat, the heat source temperature is supposed to return to that of the ambient temperature. Thus, the system must raise the temperature from the ambient temperature to the target usage temperature, that is, the net temperature lift. In addition, the gross temperature lift, including the driving temperature, is even greater. The large temperature lift leads almost directly to a decrease in the COP. There is a certain criterion of the heat pump type heat recovery system to maintain a reasonable COP. To set the criteria of recovery amount, i.e., the heating capacity of the heat pump system, the change in the COP is simulated while varying the outlet temperature of the heat source fluid.

Figure 11 plots the change in the cycle state of case III-a by decreasing the heat source fluid temperature after usage, $T_{\mathrm{src,o}}$. The evaporation pressure remarkably decreases as the after-usage heat source temperature decreases; as a result, the degree of superheat at the compressor suction side increases. Generally, the isentropic lines in the P-h diagram leans more at lower pressures and higher degrees of superheat, which indicates a large amount of compression work. Therefore, the energy consumption of the compressor increases, and the COP decreases by decreasing the after-usage heat source fluid temperature. Moreover, the degree of superheat at the inlet of the condensers increases as a result of increasing the degree of superheat at the compressor suction. This increased superheat increases the irreversible loss in the condensers as a consequence of the increased temperature difference between the pressurized water and refrigerant. This increased temperature difference is also one of the causes of the decrease in the COP.

Table 6 presents the calculation results of the COP and primary energy efficiency of cases II-c, III-a, and IV-a. The parenthesized percentages are the values relative to the COP at the standard conditions specified in Table 3. When the outlet

temperature of the heat source fluid in the evaporator is 75 °C, the waste heat is relatively abundant compared to the recovery and temperature change of the heat source fluid over the evaporator of 80 °C, which is only 5 K. The overall COP is from 8 % to 9 % higher than that at the initial conditions. When the outlet temperature is 55 °C, the temperature change of the heat source fluid is 25 K, which is 2.5 times that of the initial conditions. The COP decreases to 3.77, which is 81 % of the COP at the initial conditions; nevertheless, the primary energy efficiency is 1.4, which is still above the criteria of 1.0. The amount of waste heat strongly depends on the environment where the systems are installed; therefore, these results represent a preliminary estimate of the balance between the wasted heat and recovered heat. The above preliminary survey suggests that under the conditions where the heat source temperature after usage is maintained above 55 K, the heat recovery system of high-temperature applications is beneficial for the reduction of energy consumption.

4. CONCLUSIONS

An exploratory thermodynamic assessment of heat pump type heat recovery systems using environmentally friendly refrigerants was conducted. The coefficient of performance (COP) of the four cycle configurations used to increase the temperature of pressurized water up to 160 °C with a waste heat source of 80 °C was compared for the selected refrigerants R717, R365mfc, R1234ze(E), and R1234ze(Z). A multiple-stage "extraction" cycle drastically reduces the throttling loss in the expansion valve and the exergy loss in the condensers and, consequently, achieves the highest overall COP among the calculated cases, with refrigerant R1234ze(Z) having a critical temperature approximately equal to the target outlet water temperature. A cascade cycle using R1234ze(Z) and R365mfc results in a relatively high COP and also provides many practical benefits, such as the variety of combinations of refrigerants and lubricant oils and the prevention of the liquid back caused by a cold start. At a compressor efficiency of 0.7 and an approach temperature difference in the heat exchangers of 2 K, the calculated overall COP ranges from 4.3 to 4.94. This COP range corresponds to a primary energy efficiency of 1.62 to 1.83

when the transmission end efficiency of the electric power generation is 0.37. Even with a compressor efficiency of 0.61 and an approach temperature of 8 K, the primary energy efficiency is greater than 1.3. As described above, the thermodynamic assessment demonstrated the potential use of high-temperature heat pumps to recover waste heat as promising systems to reduce the primary energy consumption for industrial applications.

ACKNOWLEDGMENTS

The present study is sponsored by the project on the "Development of High Efficiency and Non-Freon Air Conditioning Systems" of the New Energy and Industrial Technology Development Organization (NEDO) in Japan.

REFERENCES

ASHRAE STANDARD, Designation and safety classification of refrigerants, ANSI/ASHRAE Standard 34-2007, 2008.

Akasaka, R., Higashi, Y., Miyara, A., Koyama, S., 2014. A fundamental equation of state for cis-1,3,3,3-tetrafluoropropene (R-1234ze(Z)). Int. J. Refrig., 44, 168–176.

Assaf, K., Zoughaib, A., Sapora, E., Peureux, J., Clodic, D., 2010. Experimental simulation of a heat recovery heat pump system in food industries. Proc. Int. Refirg. Air Conditioning conf. at Purdue, paper no.2311.

Bertinat, M.P., 1985. Fluids for high temperature heat pumps. Int. J. Refrig., 9, 43-50.

Bobelin, D., Bourig, A., 2012. Experimental Results of a Newly Developed Very High Temperature Industrial Heat Pump (140 ° C) Equipped With Scroll Compressors and Working. With a New Blend Refrigerant.

Brown, J.S., Zilio, C., Cavallini, A., 2009. The fluorinated olefin R-1234ze(Z) as a high-temperature heat pumping refrigerant.

Int. J. Refrig., 32, 1412-1422.

Cao, X.Q., Yang, W.W., Zhou, F., He, Y.L., 2014. Performance analysis of different high-temperature heat pump systems for low-grade waste heat recovery. Applied Thermal Engineering. 71, 1, 291–300.

Cavallini, A., Zilio, C., Brown, J.S., 2014. Sustainability with prospective refrigerants. Energy Research, 38, 285–298.

Chamoun, M., Rulliere, R., Haberschill, P., Peureux, J.L., 2014. Experimental and numerical investigations of a new high temperature heat pump for industrial heat recovery using water as refrigerant. Int. J. Refrig., 44, 177–188.

ChemSpider, CSID: 26050968, http://www.chemspider.com/Chemical-Structure.26050968.html

Domanski, P., Brown, J.S., Heo, J., Wojtusiak, J., McLinden, M.O., 2014. A thermodynamic analysis of refrigerants: Performance limits of the vapor compression cycle. International Journal of Refrigeration. 38, 71-79.

Du Pont, Formacel® 1100 Foam expansion agent Product Info, 2014, http://www2.dupont.com/Formacel/en_US /products/formacel_1100.html

Fleming, A.K., 1978. Refrigeration demands for meat processing. Int. J. Refrig., 1, 4, 217-221.

Fukuda, S., Kondou, C., Takata, N., Koyama, S, 2014. Low GWP refrigerants R1234ze (E) and R1234ze (Z) for high temperature heat pumps. Int. J. Refrig., 40, 161-173.

Honeywell Solstice 1233zd(E) Technical information, 2013, http://www.honeywell-blowingagents.com/?document=solstice - lba-technical-brochure &download=1

Hulse, R.J., Basu,R.S., Singh, R.R., Thoma, R.H.P., 2012. Physical Properties of HCFO-1233zd(E). J. Chem. Eng. Data, 57, 3581−3586.

Jakobs, R., Cibis, D., Laue, H. J., 2010. Status and outlook: Industrial heat pumps. Proc. Int. Refirg. Air Conditioning conf. at Purdue, paper no.2282.

Kew, P.A., 1982. Heat pumps for industrial waste heat recovery – a summary of required technical and economic criteria. Heat

Recovery System, 2, 3, 283-296.

Kontomaris, K.K., 2010. A Low GWP Replacement for HCFC-123 in Centrifugal Chillers: DR-2. UNEP/ASHRAE conference Road to Climate Friendly Chillers: Moving Beyond CFCs and HCFCs, Cairo, Egypt, pp. 1-10.

Koyama, S., Higashi, T., Miyara, A., Akasaka, R., 2013. JSRAE Risk Assessment of Mildly Flammable Refrigerants-2012 Progress Report, pp. 29-34.

Lemmon, E.W., Huber, M.L., McLinden, M.O., 2013. Reference Fluid Thermodynamic and Transport Properties - REFPROP Ver. 9.1. National Institute of Standards and Technology, Boulder, CO, USA.

Loh, G., Creazzo, J.A., Robin, M.L., 2010. Further Development of FEA-1100: a low GWP Foam Expansion Agent. Proc. Polyurethanes 2010 Technical Conference, Houston, TX, USA.

Matrix Scientific MSDS, 2010. http://www.matrixscientific.com/1h1h2h-heptafluoropent-1-ene-mfcd00039253-71164-40 -4-c5h3f7.html

McLinden, M.O., Kazakov, A.F., Brown, J.S., Domanski, P.A., 2014. A Thermodynamic Analysis of Refrigerants: Possibility and Tradeoffs for Low-GWP refrigerants. Int. J. Rerfirg., 38, 80-92.

Myhre, G., Shindell, D., Bréon, F.M., Collins, W., Fuglestvedt, J., Huang, J., Koch, D., Lamarque, J.F., Lee, D., Mendoza, B., Nakajima, T., Robock, A., Stephens, G., Takemura, T., Zhang, H., 2013. Chapter 8 Anthropogenic and Natural Radiative Forcing. IPCC 2013 Assessment Report 5th Climate Change - The Physical Science Basis, the Intergovernmental Panel on Climate Change [Stocker, T.F., D. Qin, G.-K. Plattner, M. Tignor, S.K. Allen, J. Boschung, A. Nauels, Y. Xia, V. Bex and P.M. Midgley (eds.)]. Cambridge University Press, Cambridge, United Kingdom and New York, NY, USA.

Pearson, S.F., 1999. Ammonia refrigeration systems. ASHRAE Journal, 41, 3, ProQuest Central, 24-29.

Rattner, A.S., Garimella, S., 2011. Energy harvesting, reuse and upgrade to reduce primary energy usage in the USA. Energy, 36, 10, 6172–6183.

Solvay Product Safety Summary of 1,1,1,3,3-pentafluorobutane, 2011. http://www.icca-chem.org/Portal/SafetySummary Sheets /634590375264467619 _PSS%20HFC-365mfc_V02.pdf

SynQuest MSDS, 2012. SynQuest Laboratories, Inc., http://www.synquestlabs.com/msds/1300-7-09.pdf

U.S. Department of Energy, 2003. Industrial Heat Pumps for Steam and Fuel Savings. http://www1. eere.energy.gov /manufacturing/tech_assistance/pdfs/heatpump.pdf, pp. 1-15.

U.S. Department of Energy, 2008. Waste Heat Recovery: Technology and Opportunities in U.S. Industry, https:// www1.eere.energy.gov/manufacturing/intensiveprocesses/pdfs/waste_heat_recovery.pdf, pp.12-24.

Zhang, W., Yang, Z.Q., Lu, J., Lu, J., 2013. Vapor Pressures of 2-Chloro-3,3,3-trifluoropropene (HCFO-1233xf). J. Chem. Eng. Data, 58, 2307–2310.

Figure Captions

Figure 1 Theoretical COP of a basic heating cycle allows large subcooling for selected refrigerants (ΔT_{liftG} = 80 K, SC = 60 K, SH = 3 K, η_{compr}= 1.0). The notations "ze(E)" and "ze(Z)" refer to R1234ze(E) and R1234ze(Z), respectively.

(a) calculation model

(b) theoretical COP

(c) pressure ratio

(d) volumetric heating capacity

Figure 2 Proposed cycle configurations for the heat recovery system

(a) case I: triple tandem cycle

(b) case II: two-stage extraction cycle

(c) case III: three-stage extraction cycle

(d) case IV: cascade cycle

Figure 3 Model for the approach temperature and pinch points in the heat exchangers

Figure 4 State of the cycle: case I with R1234ze(E), R1234ze(E), and R365mfc

Figure 5 State of the cycle: case II-c with R1234ze(Z) and R365mfc

(a) *P-h* diagram of the low-temperature side cycle

(b) *T-s* diagram of the low-temperature side cycle

(c) *P-h* diagram of the high-temperature side cycle

(d) *T-s* diagram of the high-temperature side cycle

Figure 6 State of the cycle: case III-a with R1234ze(Z)

(a) P-h diagram

(b) T-s diagram

Figure 7 State of the cycle: case IV-a with R1234ze(Z) and R365mfc

(a) P-h diagram

(b) T-s diagram

Figure 8 Variation in the overall COP versus the change in the operation conditions

(a) case III-a

(b) case IV-a

Figure 9 Effects of the compressor efficiency on the cycle state of case III-a

(a) P-h diagram

(b) T-s diagram

Figure 10 Effects of the heat exchanger size on the cycle state of case III-a

(a) P-h diagram

(b) T-s diagram

Figure 11 Effects of the heat source fluid temperature in the evaporator on the cycle state of case III-a

(a) P-h diagram

(b) T-s diagram

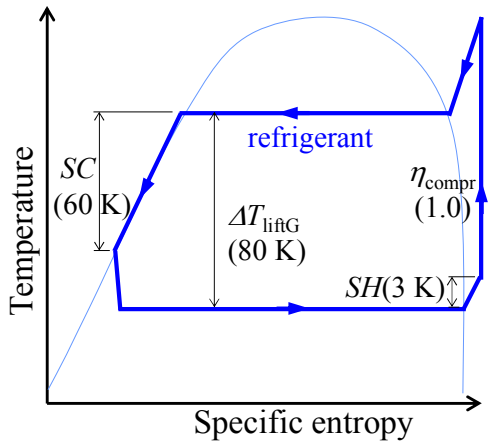

(a) calculation model

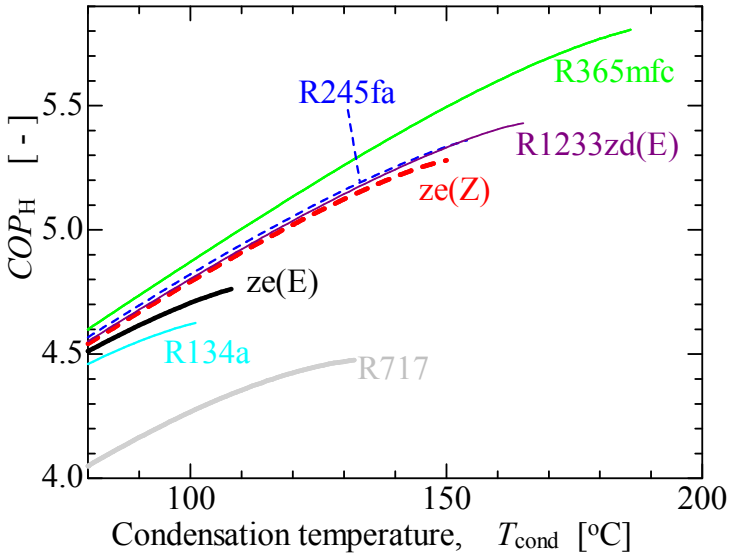

(b) theoretical COP

Figure 1 Theoretical COP of a basic heating cycle allows large subcooling for selected refrigerants (ΔT_{liftG} = 80 K, *SC* = 60 K, *SH* = 3 K, η_{compr}= 1.0). The notations "ze(E)" and "ze(Z)" refer to R1234ze(E) and R1234ze(Z), respectively.

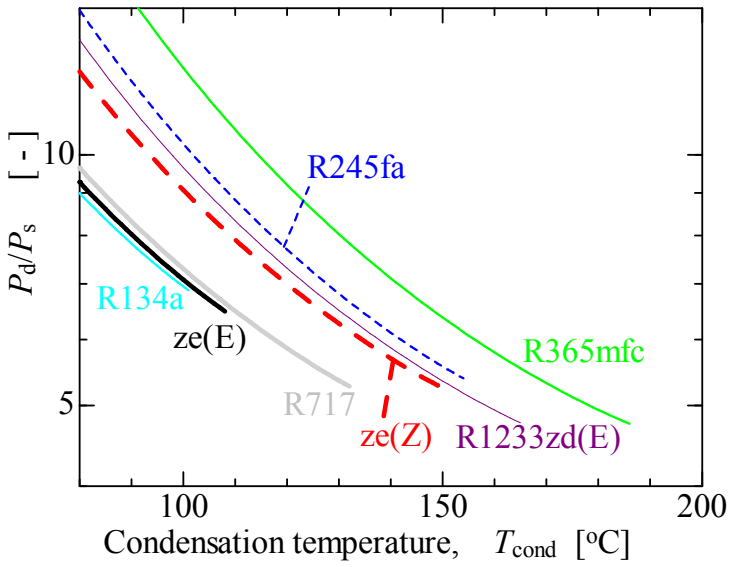

(c) pressure ratio

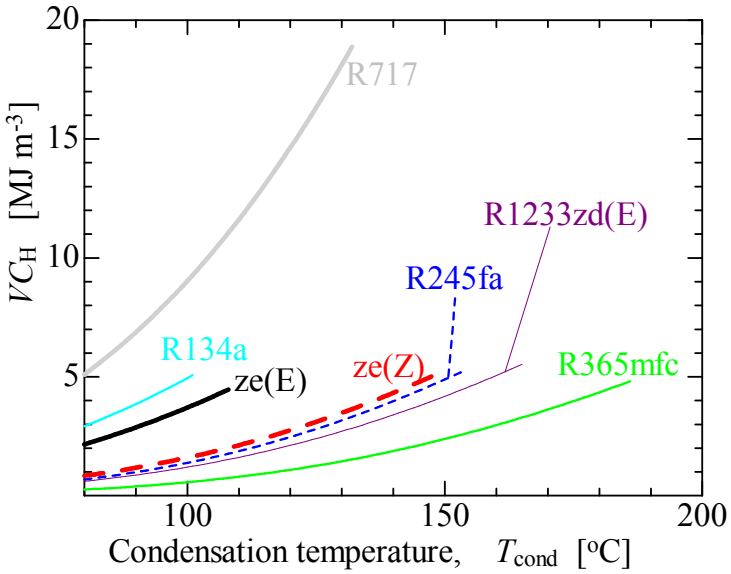

(d) volumetric heating capacity

Figure 1 Continued

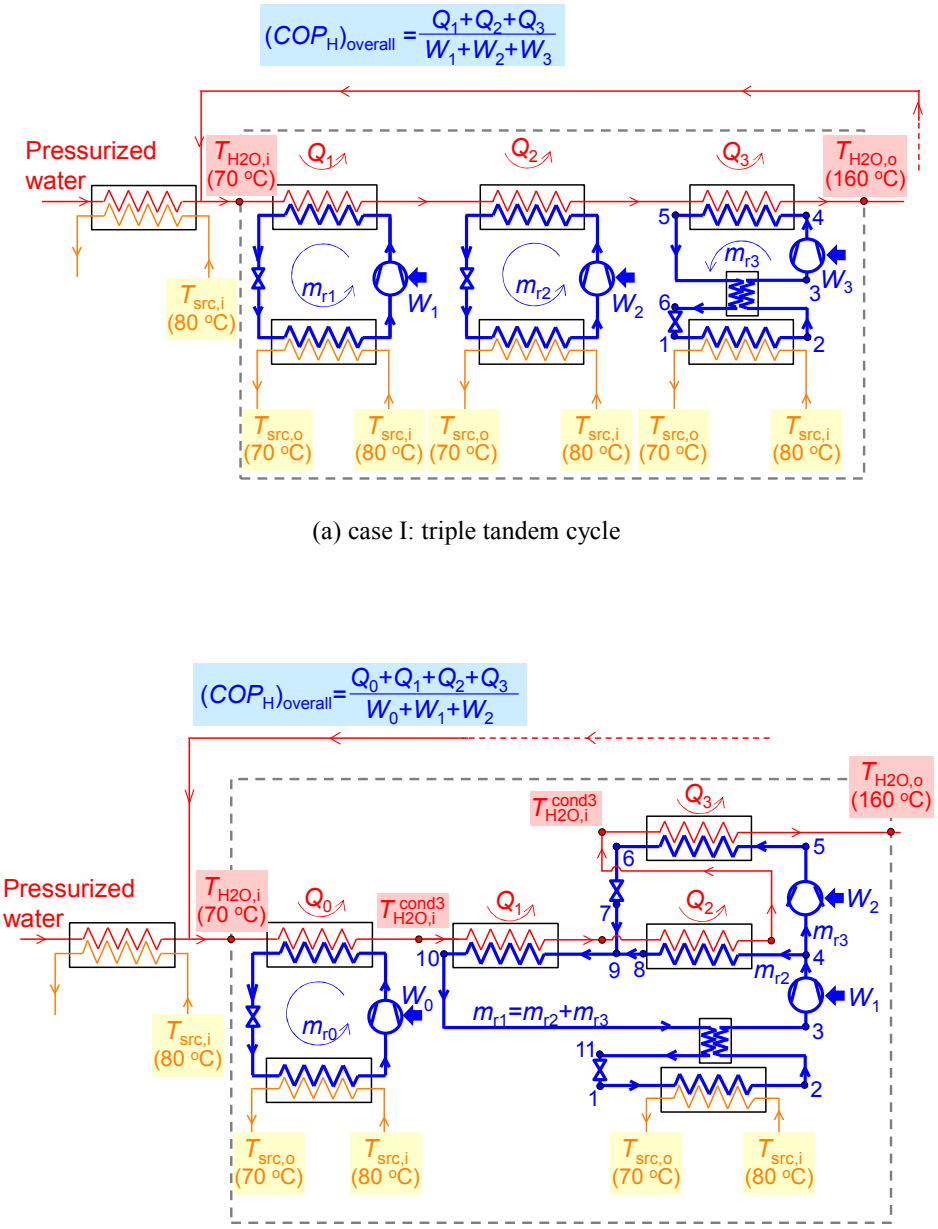

(a) case I: triple tandem cycle

(b) case II: two-stage extraction cycle

Figure 2 Proposed cycle configurations for the heat recovery system (parenthesized temperatures denote the standard conditions listed in Table 3).

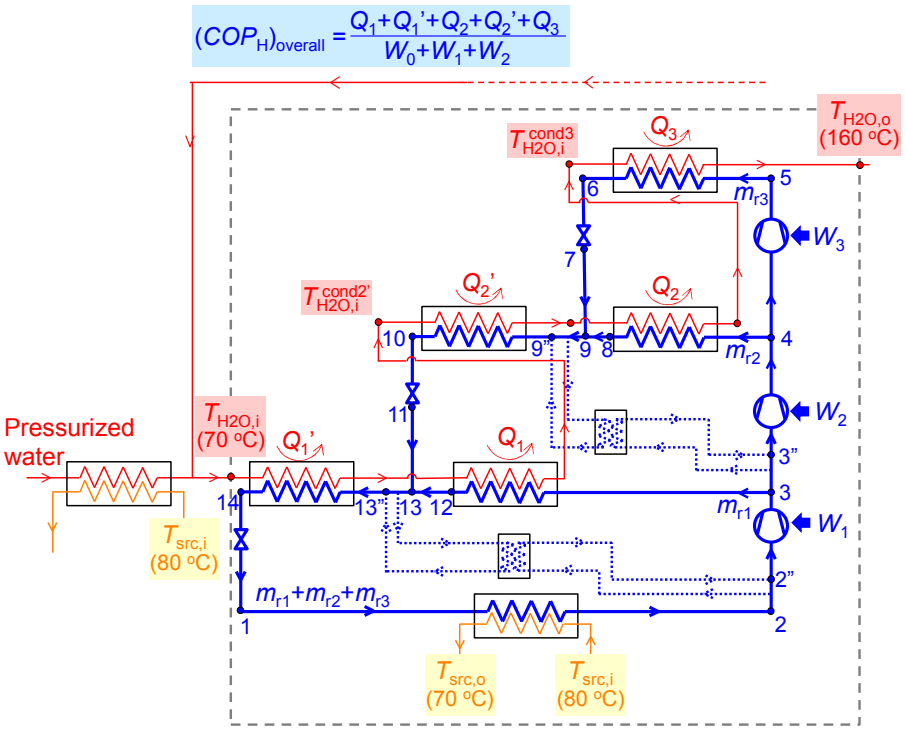

(c) case III: three-stage extraction cycle

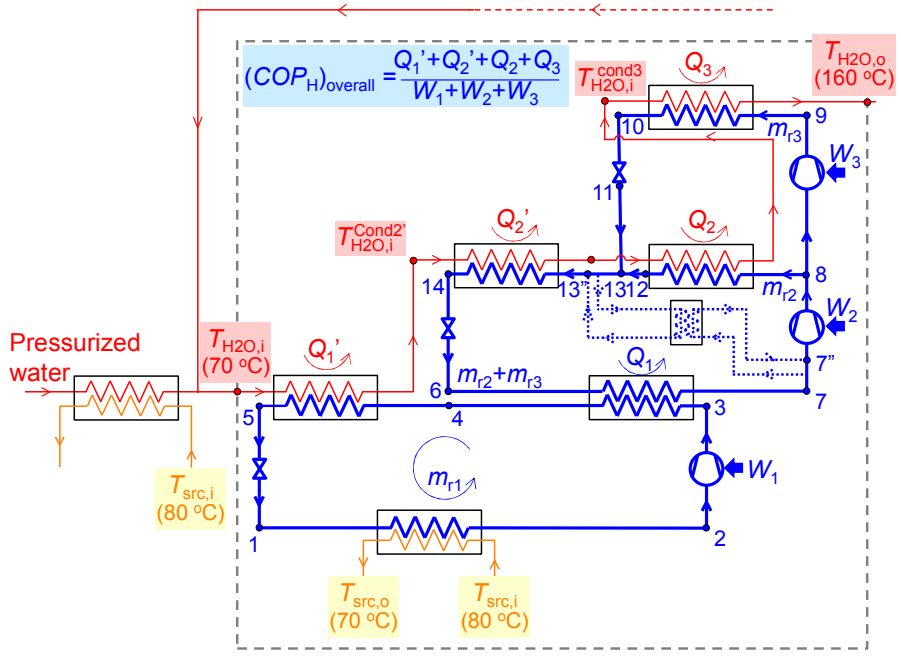

(d) case IV: cascade cycle

Figure 2 continued

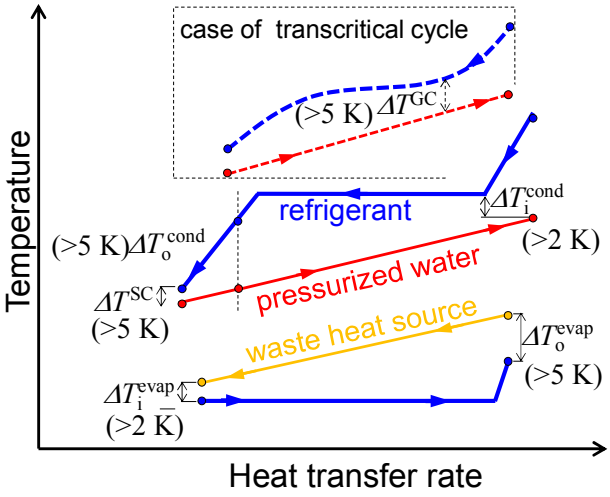

Figure 3 Model for the approach temperature and the pinch points in the heat exchangers (parenthesized temperatures denote the standard conditions listed in Table 3).

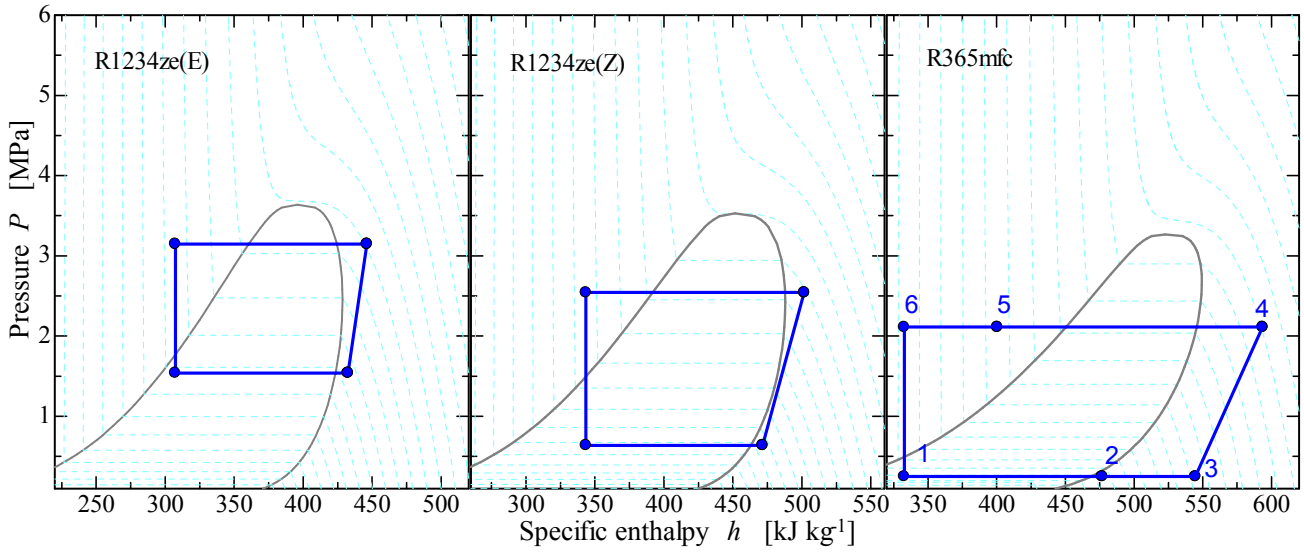

(a) *P-h* diagram

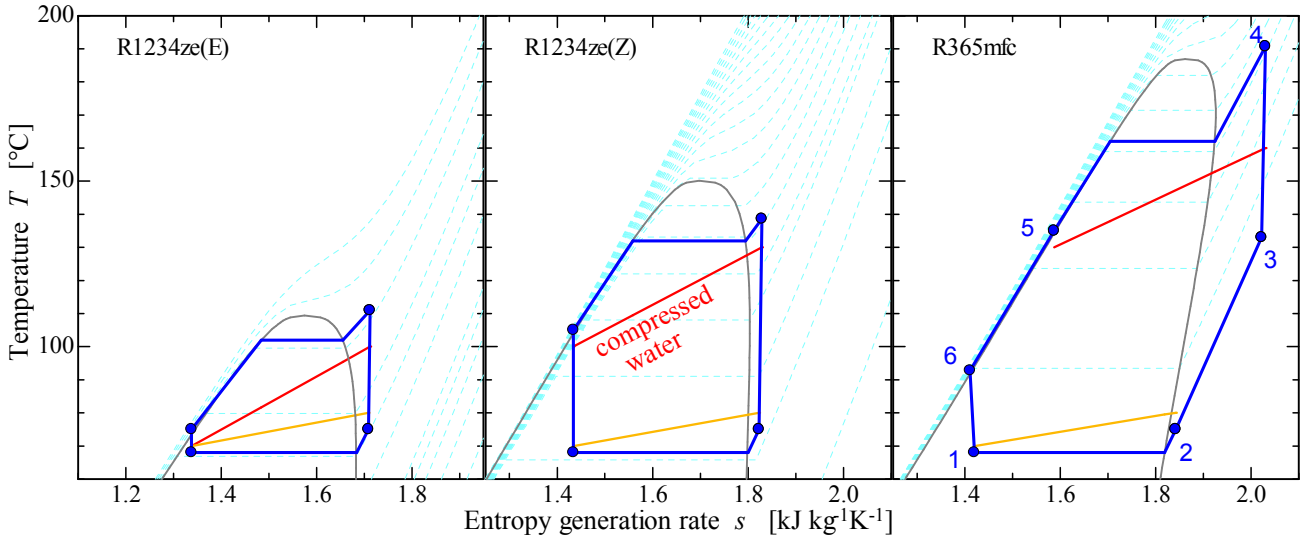

(b) *T-s* diagram

Figure 4 State of the cycle: case I with R1234ze(E), R1234ze(E), and R365mfc

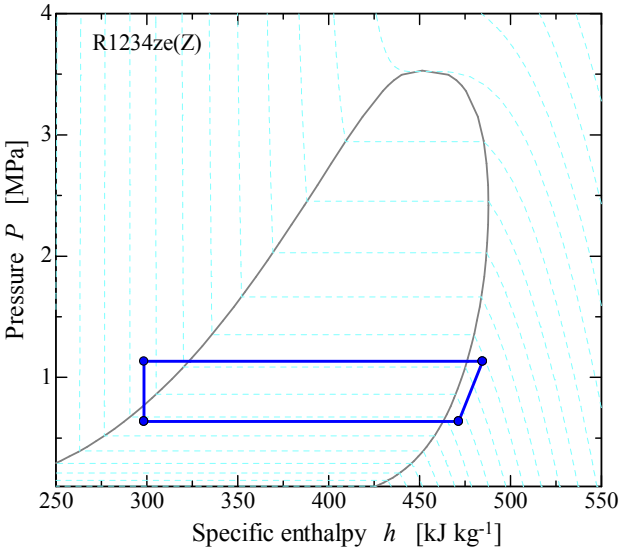

(a) *P-h* diagram of the low-temperature side cycle

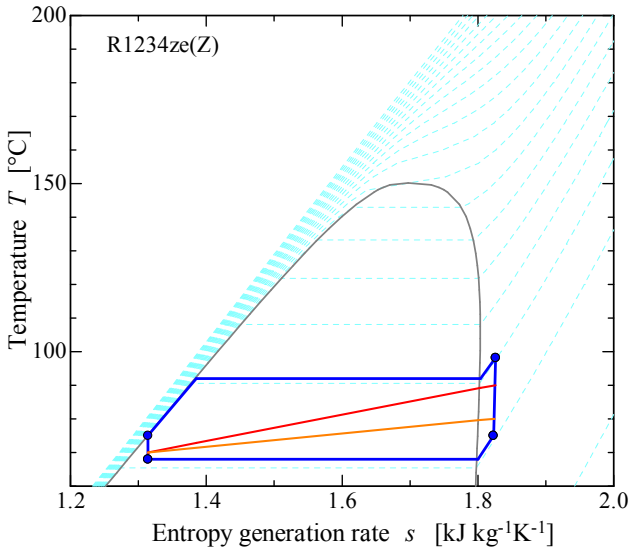

(b) *T-s* diagram of the low-temperature side cycle

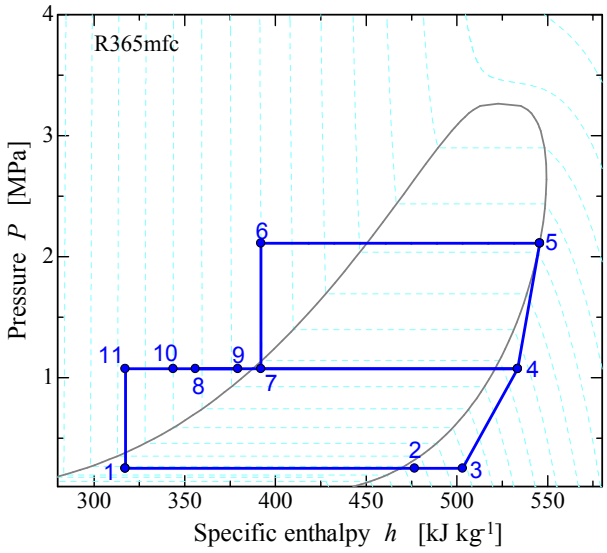

(c) *P-h* diagram of the high-temperature side cycle

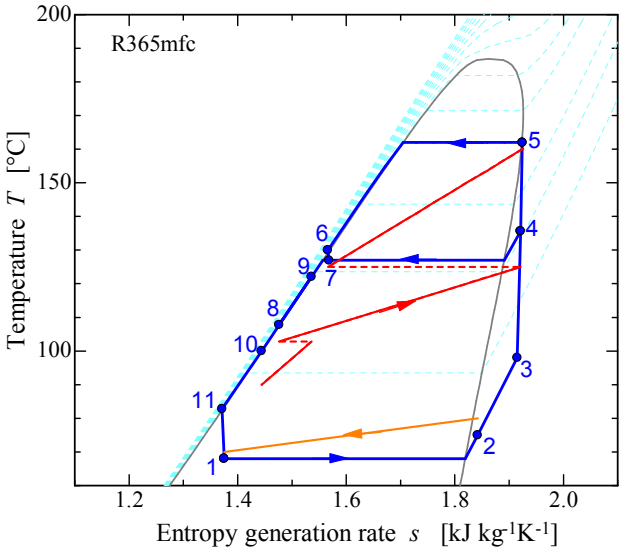

(d) *T-s* diagram of the high-temperature side cycle

Figure 5 State of the cycle: case II-c with R1234ze(Z) and R365mfc

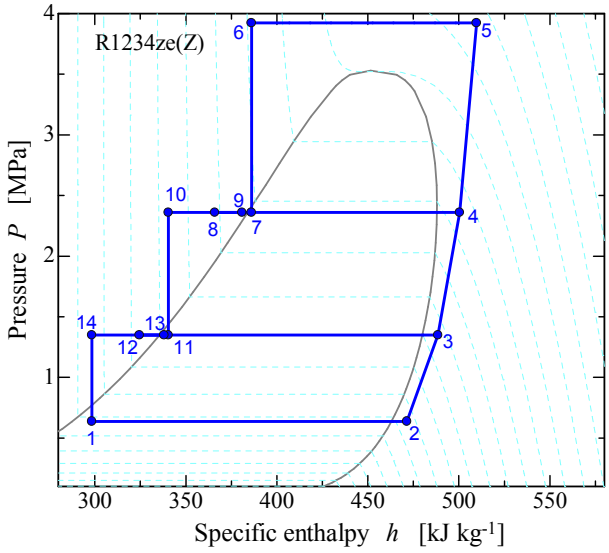

(a) *P-h* diagram

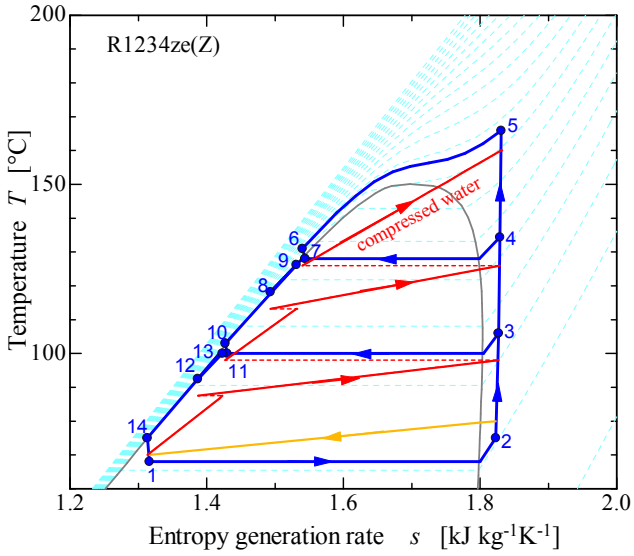

(b) *T-s* diagram

Figure 6 State of the cycle: case III-a with R1234ze(Z)

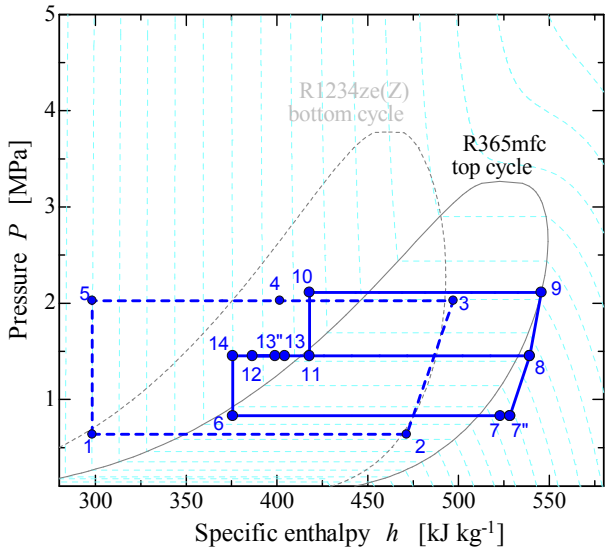

(a) *P-h* diagram

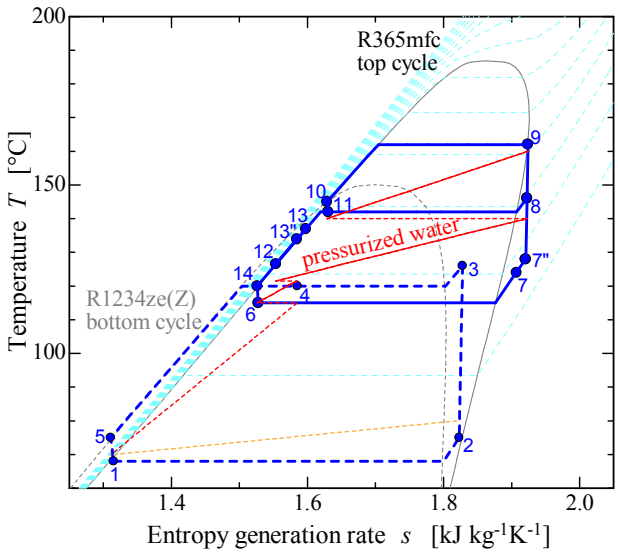

(b) *T-s* diagram

Figure 7 State of the cycle: case IV-a with R1234ze(Z) and R365mfc

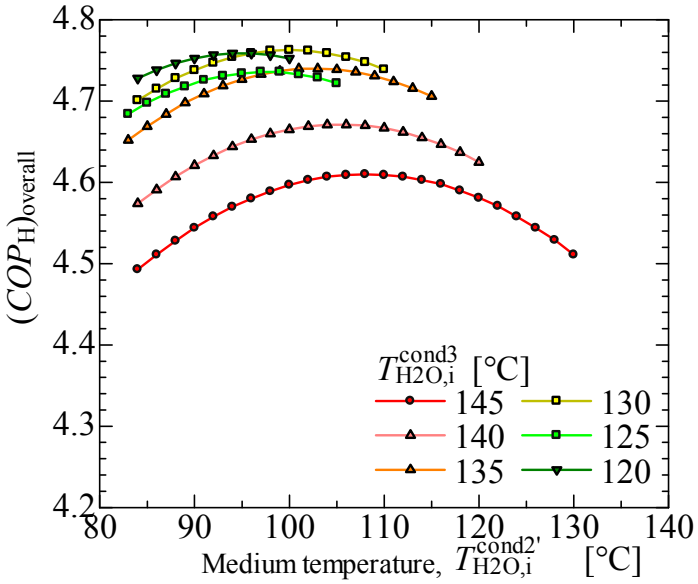

(a) case III-a

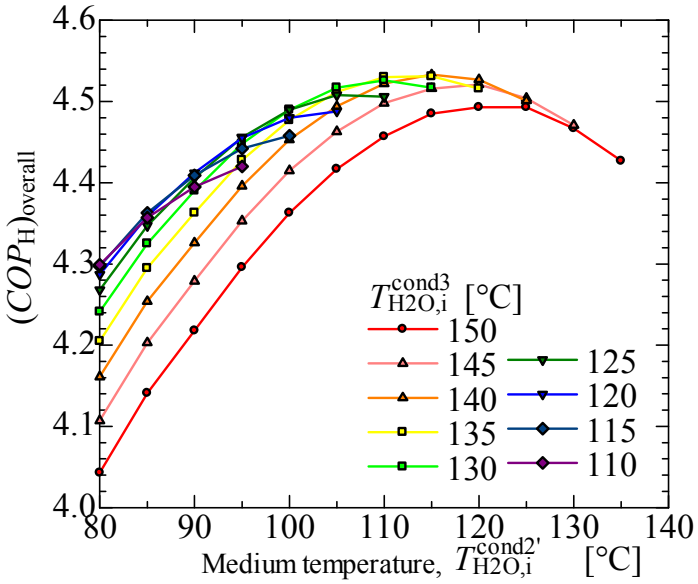

(b) case IV-a

Figure 8 Variation in the overall COP versus the change in the operation conditions

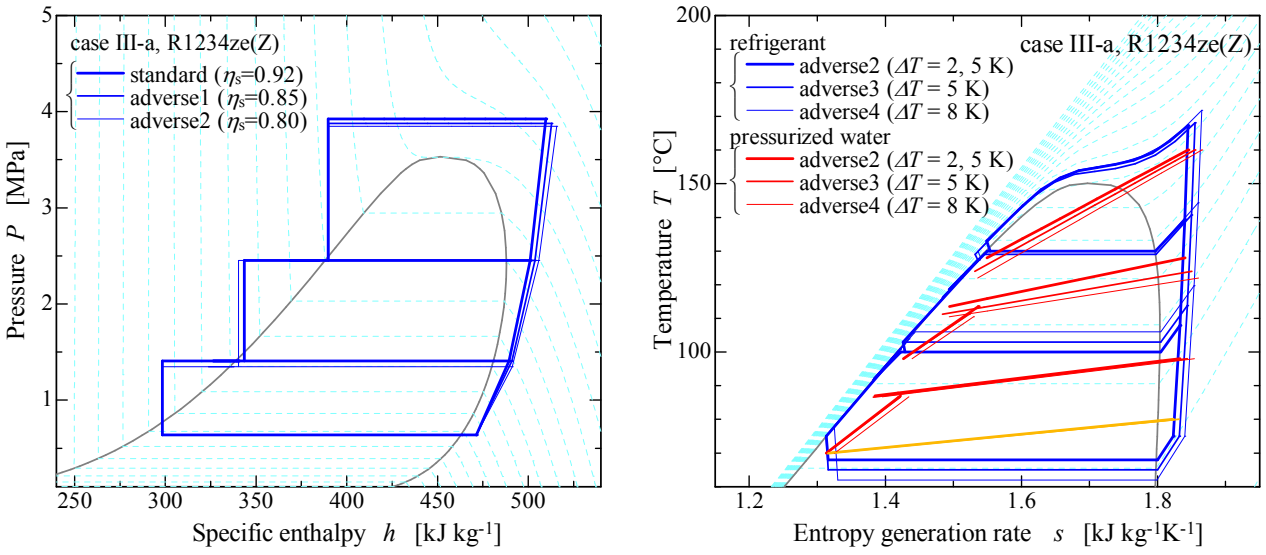

(a) *P-h* diagram (b) *T-s* diagram

Figure 9 Effects of the compressor efficiency on the cycle state of case III-a

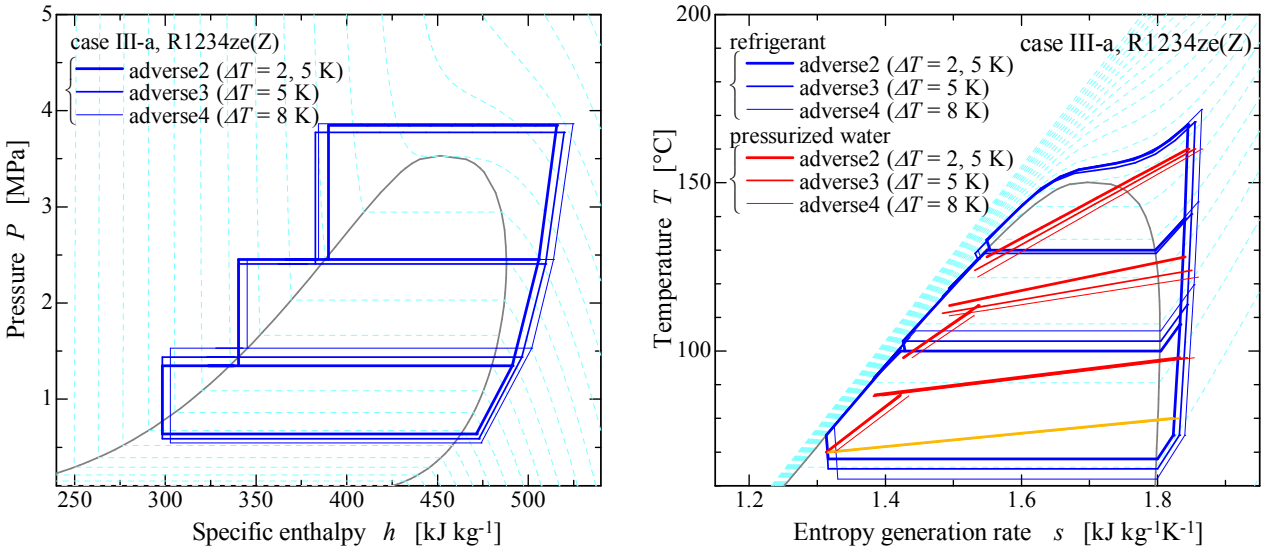

(a) *P-h* diagram (b) *T-s* diagram

Figure 10 Effects of the heat exchanger size on the cycle state of case III-a

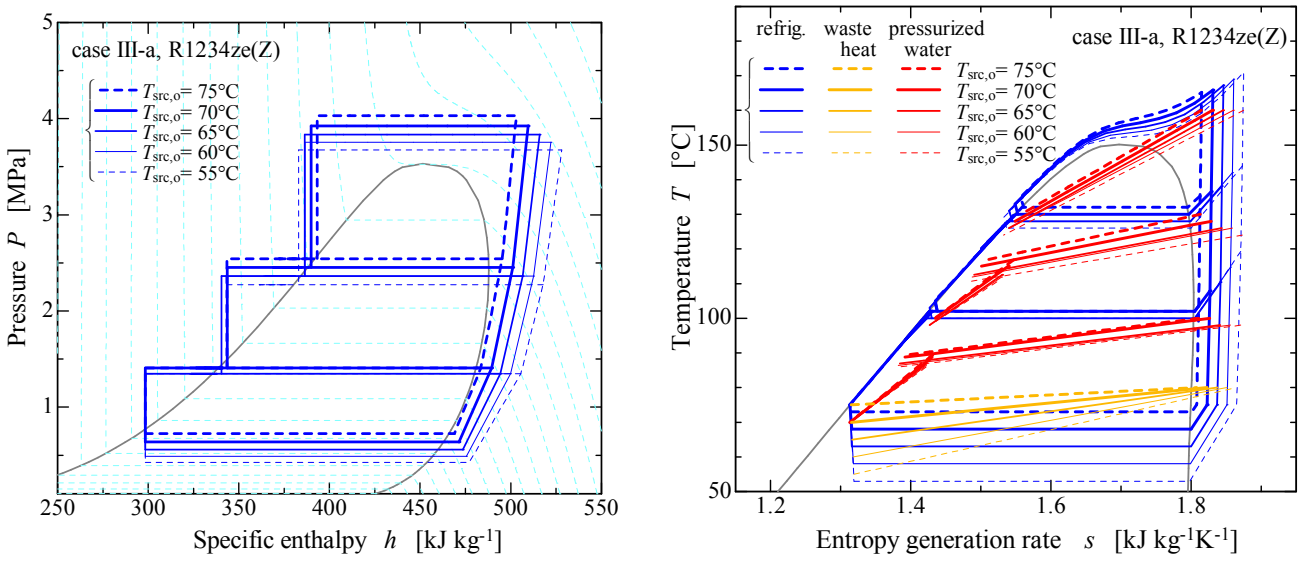

(a) *P-h* diagram

(b) *T-s* diagram

Figure 11 Effects of the heat source fluid temperature in the evaporator on the cycle state of case III-a

Table 1 Fundamental characteristics of candidate refrigerants for heat pump type waste heat recovery system

	R134a	R1234ze(E)	R717	R1234ze(Z)	R245fa	R1233zd(E)	R365mfc
Formula	CH_2FCF_3	$CHF=CHCF_3$ (trans)	NH_3	$CHF=CHCF_3$ (cis)	$C_3H_3F_5$	$CF_3CH=CClH$ (trans)	C_4H_5F
CAS number	811-97-2	29118-24-9	7664-41-7	29118-25-0	460-73-1	102687-65-0	406-58-6
Molar mass [g mol^{-1}]	102.0	114.0	17.0	114.0	134.05	130.5	148
ODP	0	0	0	0	0	slight	0
GWP_{100}	1300 [a)]	< 1 [a)]	0 [a)]	< 1 [a)]	858 [a)]	1 [f)]	804 [a)]
Safety classification [b)]	A1	A2L	B2	A2L [d)] (expected)	B1	A1 [f)] (expected)	A2 [h)] (expected)
Normal boiling point[°C] [c)]	-26.1	-19.0	-33.3	9.8[e)]	15.1	18.3	40.2
P_{crit} [MPa] [c)]	4.06	3.64	11.33	3.53 [e)]	3.65	3.77 [g)]	3.27
T_{crit} [°C] [c)]	101.1	109.4	132.3	150.1 [e)]	154.0	165.6 [g)]	186.9

a) IPCC 5th report, chapter 8 (Myhre *et al.*, 2013)

b) ANSI/ASHRAE standard 34-2007 (A-Non-toxic, B-Toxic; 1-Non-flammable, 1L- Mildly flammable, 2-Flammable)

c) REFPROP 9.1 (Lemmon *et al.*, 2013)

d) Koyama *et al.* (2013)

e) Akasaka *et al.* (2014)

f) Honeywell solstice 1233zd(E) Technical information (2013)

g) Hulse *et al.* (2012)

h) Solvay Product Safety Summary of 1,1,1,3,3-pentafluorobutane (2011)

Table 2 Alternative low-GWP refrigerants for R365mfc

	Formula	CAS number	ODP	GWP	Normal boiling point [°C]	Safety classification [d]	Molar mass [g mol^{-1}]
R1233xf	$CF_3CCl=CH_2$	2730-62-3	slight [c]	low [c]	12 [e]	A1(expected) [b]	130.5
R1336mzz(Z)	$CF_3CH=CHCF_3$(cis)	692-49-9	0 [c]	2 [a]	33 [f] [i]	A1(expected) [f] [i]	164.05
R1447fz	$CF_3CF_2CF_2CH=CH_2$	355-08-8	0 [c]	low [c]	32 [g]	A3(expected) [g]	196.07
R1438mzz(E)	$CF_3CH=CHCF_2CF_3$(trans)	935553-90-5	0 [c]	low [c]	30 [h]	-	214.06

a) IPCC 5th report chapter 8 (Myhre *et al.*, 2013)

b) SynQuest MSDS (2012)

c) Loh *et al.* (2010)

d) ANSI/ASHRAE standard 34-2007 (A-Non-toxic, B-Toxic; 1-Non-flammable, 1L- Mildly flammable, 2-Flammable)

e) Zhang *et al.* (2012)

f) Du Pont Formacel® 1100 Product Information (2014)

g) Matrix Scientific MSDS (2010)

h) ChemSpider, CSID:26050968

i) Kontomaris (2010)

Table 3 Typical calculation conditions for the case study (standard condition)

Pressurized water (1 MPa)	inlet temp. (after pre-heating)	$T_{H2O,i}$	70 °C
	outlet temp.	$T_{H2O,o}$	160 °C
Heat source	inlet temp.	$T_{src,i}$	80 °C
	outlet temp.	$T_{src,o}$	70 °C
Compressor	isentropic efficiency	η_s	0.92
	mechanical efficiency	η_{mech}	0.85
	motor efficiency	η_{motor}	0.90
Evaporator	pinch temp. at the entrance	ΔT_i^{evap}	> 2 K
	pinch temp. at the exit	ΔT_o^{evap}	> 5 K
Condenser	pinch temp. at the entrance	ΔT_i^{cond}	> 2 K
	pinch temp. at the exit	ΔT_o^{cond}	> 5 K
Gas cooler	pinch temp.	ΔT^{GC}	> 5 K
Subcooler	pinch temp.	ΔT^{SC}	> 5 K
Internal heat exchanger	pinch temp.	ΔT^{IH}	> 2 K
Cascade condenser	saturation temp. difference	$T_{cond}^{cascade} - T_{evap}^{cascade}$	5 K
	pinch temp.	$\Delta T^{cascade}$	> 2 K

Table 4 Typical calculation results for a delivery temperature 160 °C with a heat source of 80 °C under the standard conditions listed in Table 3

case	$T_{H2O}1$ [°C] / refrigerant1 / COP1 [-] / VC1 [MJ m^{-3}] / P_d/P_s1 [-]	$T_{H2O}2$ [°C] / refrigerant2 / COP2 [-] / VC2 [MJ m^{-3}] / P_d/P_s2 [-]	$T_{H2O}3$ [°C] / refrigerant3 / COP3 [-] / VC3 [MJ m^{-3}] / P_d/P_s3 [-]	overall COP, $(COP_H)_{overall}$	primary energy efficiency, η_{pe}
I	70 to 100 / R1234ze(E) / 7.731 / 11.34 / 2.05	100 to 130 / R1234ze(Z) / 4.01 / 4.71 / 3.99	130 to 160 / R365mfc / 3.02 / 2.22 / 8.43	4.22	1.56
II-a	70 to 90 / R1234ze(E) / 10.18 / 11.00 / 1.68	90 to 122 / R1234ze(Z) / 4.01 / - / 3.43	122 to 160 / 1.66	4.63	1.71
II-b	70 to 90 / R1234ze(Z) / 10.81 / 5.55 / 1.78	90 to 121 / R1234ze(Z) / 4.01 / - / 3.37	121 to 160 / 1.66	4.65	1.72
II-c	70 to 90 / R1234ze(Z) / 10.81 / 5.55 / 1.78	90 to 125 / R365mfc / 3.96 / - / 4.29	125 to 160 / 1.97	4.61	1.71
III-a	70 to 98	98 to 126 / R1234ze(Z) / 4.77 / - / 1.75	126 to 160 / 1.66	4.77	1.76
III-b	70 to 102	102 to 133 / R1233zd(E) / 4.73 / - / 1.84	133 to 160 / 1.60	4.73	1.75
III-c	70 to 98	98 to 122 / R365mfc / 4.71 / - / 1.72	122 to 160 / 2.09	4.71	1.74
IV-a	70 to 115 / R1234ze(Z) / 3.07 / 3.08 / 3.18	115 to 140 / R365mfc / 8.51 / - / 1.75	140 to 160 / 10.97 / 1.45	4.53 (temperature in the cascade condenser, 115 °C)	1.68
IV-b	70 to 87 / R717 / 2.06 / 5.23 / 1.69	87 to 126 / R365mfc / 6.01 / - / 2.59	123 to 160 / 9.88 / 1.93	4.43 (temperature in the cascade condenser, 92 °C)	1.64

Table 5 Effects of the compressor efficiency and heat exchanger size (parenthesized percentages are relative COPs based on the COP at the standard conditions)

		standard condition	adverse condition 1	adverse condition 2	adverse condition 3	adverse condition 4
conditions	η_s	0.92	0.85	0.80	→	→
	η_{mech}	0.85	→	→	→	→
	η_{motor}	0.90	→	→	→	→
	η_{compr}	0.70	0.65	0.61	→	→
	ΔT_i^{EVAP}	> 2.0 K	→	→	> 5.0 K	> 8.0 K
	ΔT_o^{evap}	> 5.0 K	→	→	→	> 8.0 K
	ΔT_i^{COND}	> 2.0 K	→	→	> 5.0 K	> 8.0 K
	ΔT_o^{cond}	> 5.0 K	→	→	→	> 8.0 K
	ΔT^{GC}	> 5.0 K	→	→	→	> 8.0 K
	ΔT^{SC}	> 5.0 K	→	→	→	> 8.0 K
	ΔT^{IH}	> 2.0 K	→	→	> 5.0 K	> 8.0 K
overall COP, $(COP_H)_{overall}$	case II-c	4.61 (100%)	4.31 (94%)	4.18 (91%)	3.88 (84%)	3.56 (77%)
	case III-a	4.77 (100%)	4.46 (94%)	4.25 (89%)	4.01 (84%)	3.67 (77%)
	case IV-a	4.53 (100%)	4.25 (94%)	4.05 (89%)	3.81 (84%)	3.43 (76%)
primary energy efficiency, η_{pe}	case II-c	1.70	1.60	1.54	1.44	1.32
	case III-a	1.76	1.65	1.57	1.48	1.36
	case IV-a	1.68	1.57	1.50	1.41	1.27

Table 6 Effects of the temperature change of the heat source fluid in the evaporator (parenthesized percentages are relative COPs based on the COP at the standard conditions)

		favorable condition	standard condition	adverse condition 1	adverse condition 2	adverse condition 3
conditions	$T_{src,i} \rightarrow T_{src,o}$	80→75 °C	80→70 °C	80→65 °C	80→60 °C	80→55 °C
	ΔT_{src}	5 K	10 K	15 K	20 K	25 K
overall COP, $(COP_H)_{overall}$	case II-c	4.98 (108%)	4.61 (100%)	4.26 (92%)	3.96 (86%)	3.67 (80%)
	case III-a	5.19 (109%)	4.77 (100%)	4.40 (92%)	4.07 (85%)	3.79 (80%)
	case IV-a	4.92 (109%)	4.53 (100%)	4.20 (93%)	3.91 (86%)	3.64 (80%)
primary energy efficiency, η_{pe}	case II-c	1.84	1.70	1.57	1.46	1.36
	case III-a	1.92	1.76	1.63	1.51	1.40
	case IV-a	1.82	1.68	1.55	1.45	1.35